Wavelet transform: A tool for the interpretation of upper mantle converted phases at high frequency

Julie Castillo, A. Mocquet, Ginette Saracco

HAL Id: hal-01767215
https://hal.science/hal-01767215

Wavelet transform : A tool for the interpretation of upper mantle converted phases at high frequency

Julie Castillo, Antoine Mocquet,

Laboratoire de Planétologie et Géodynamique, Nantes University, France.

Ginette Saracco [1]

Laboratoire de Géosciences, Rennes University, France.

Abstract. P to S converted receiver functions recorded at VBB FDSN California stations are studied in the frequency range of 0.1 to 1 Hz. Microseismic noise is maximum in this frequency range, but signal processing by the wavelet transform enables us: (1) to enhance seismic phases associated with seismic velocity gradients and discontinuities at the base of the upper mantle, (2) to extract accurate arrival times, and (3) to obtain an accurate insight into the frequency content. In the case of California, one seismic discontinuity and two zones of high gradients in the depth range of 625 to 720km are recurrently observed for two different data sets.

Introduction

Many studies have focused on the interface between the upper and the lower mantle of the convective Earth. The diversity of seismic phases and frequency ranges used for the interpretation has lead to the construction of different models. The most commonly used model consists of a less than 5-km thick discontinuity (e.g. *Paulssen* [1985]) which is situated at a depth of 660km in spherically symmetric Earth models, hereafter abbreviated as SSEM (e.g. ak135, [*Kennett et al.*, 1995]). Mineral physics indicates that the depth at which this seismic discontinuity occurs varies inversely with respect to lateral variations of temperature, due to the endothermic transformation of ringwoodite (γ-phase) into perovskite (Pv) and magnesiowustite (Mw) (e.g. *Ito and Takahashi* [1989]). Studies also predict the presence of high velocity gradients which should be associated with the transformation of non-olivine minerals (i.e. garnet and ilmenite) [*Vacher et al.*, 1998]. These results support the opinion that the seismic velocity and density jump introduced in SSEM at a depth of 660km should only be regarded as the simplest expression of a more complicated pattern of multiple high gradients and discontinuities. Although the impedance contrast associated with the transformation of non-olivine components is predicted to be 6 times smaller than the one associated with the transformation of olivine phases, observations by *Niu and Kawakatsu* [1996] under Japan and China, and *Simmons and Gurrola* [2000] under California, suggest that the former transformations might be detected

by seismological means. Since the amplitude of a converted phase depends on the ratio between the width of the interface and the wavelength, the frequency content of dispersed waveforms provides information on the smoothness of seismic discontinuities. High seismic gradients related to non-olivine transformations are 10 to 50km thick; thus, P to S converted phases (Pds) should be studied at frequencies higher than 0.1Hz. However, in this particular frequency range, the microseismic coherent noise has maximum energy. Numerous global studies of the 660km interface have been conducted at frequencies lower than 0.17Hz in order to remove this noise (see [*Chevrot et al.*, 1999] for a review), but they exhibit a radial resolution worse than 30km. In this paper, we apply the wavelet transform to high frequency (0.1-1Hz) deconvolved Pds Very Broad Band (VBB) waveforms. This data processing technique, which has been used in various geophysical fields (e.g., [*Paulssen*, 1985; *Kumar et al.*, 1997; *Moreau et al.*, 1999; *Valéro*, 2000]), makes it possible for us: (1) to detect accurately the arrival time of seismic phases converted at sharp (less than 10km thick) discontinuities (2) to highlight waveforms generated through high seismic gradients and derive their frequency content, and consequently (3) to improve the radial resolution of seismic models close to the 660km depth range. The efficiency of the method is discussed using VBB data recorded at 3 FDSN California stations.

Data processing

We convolve the discrete complex Morlet wavelet (e.g. *Morlet et al.*, [1982]) with the studied signal, in the frequency range 0.1 to 1Hz to obtain its energy and phase diagram. Thus we can expect a radial resolution bounded by 6 and 60km, roughly. Exploiting different values of the non-dimensional gaussian width of the wavelet σ illuminates complementary information: high values ($\sigma > 1$) provide a better resolution in the frequency domain while smaller values favor the accurate detection of arrival times. An initial data set of 138 three-component seismograms generated between 1991 and 1996 in the Tonga subduction zone – in the magnitude range of 5.5 to 7, and depth ranges of 0-70km and 400-680km – has been constructed with epicentral distances contained between 65 and 85deg. for the 3 stations under study (figure 1a). Only events displaying a signal to noise (S/N) ratio greater than 10 for the P-wave arrival on the longitudinal component are of interest. Biases introduced by azimuthal anisotropy [*Montagner*, 1998] are reduced by restricting the backazimuthal aperture to ± 10 degrees. The latter constraints define a final data set of 52 three compo-

---

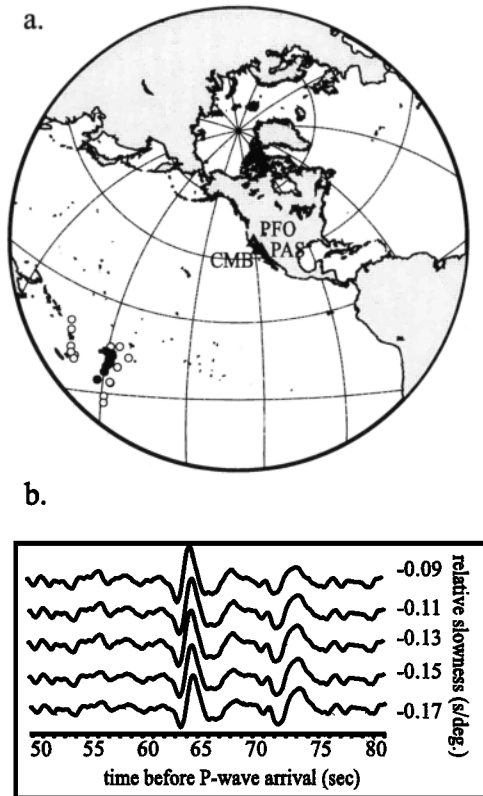[1] Now at Laboratoire Cerege, Aix-Marseille, France.

a.

b.

Figure 1. (a) Stations (triangles) and events used in this study. Black circles : deep events (hypocenter depth greater than 450km) ; white circles : shallow events (hypocenter depth smaller than 70km). (b) Stacked receiver functions as a function of slowness. Slowness values are relative to the one of the direct P-wave.

nent traces. Two subsets are constructed in order to detect possible artifacts induced by heterogeneities in the source region, and to test the redundancy of the interpretation in terms of mantle structure. The subsets consist of 34 shallow events (focal depth h shallower than 70km), and 18 deep events (h $\geq$ 400km), respectively. The stacked receiver functions are obtained using *Vinnik*'s [1977] method for a reference distance of 75deg. The time window of the deconvolving P-wave is tested in the range 10 to 40s. The slowness

values of the normal move-out corrections are tested in the range (-0.09 , -0.17) s.deg^{-1} (figure 1b). Figure 3 is focused on P to S conversions at 660km depth. Between 53 and 75sec, the maximum error on arrival times is lower than ±0.3sec. The energy level of the post-stack noise sampled before the P-wave arrival is illustrated in figure 2. In the frequency range 0.1-1.0Hz, the noise energy level is dominated by the coherent microseismic noise at 0.25Hz (figure 2a). Deconvolution and stacking serve to increase the S/N ratio and spread out the noise level distribution over all the frequency range (figure 2b). The S/N ratio is close to 2.5 for the stack of the 52 SV-components, while it is lower than 0.5 for individual traces. This effect is important for further signal interpretation, since 0.2-0.4Hz is the frequency range in which waves generated on upper mantle seismic gradients are expected to reach maximum energy.

Results

The stacked deconvolved Pds traces are shown in figures 3a and 3b, respectively for deep and shallow events. Several packets stand out of the time frequency energy diagram. The features common to both stacks are described first. The energy maximum arrives with a time lag of ±3s with respect to the P660s arrival time predicted by ak135. Two additional maxima are observed between 0.3 and 0.5Hz. The arrival times of the latter are around 66s, and 73s, respectively. Among the three successive arrivals, only the second one displays a significant dispersion over a 4s wide time window, indicating a 20km thick structure. The first and third phases are sharp and non-dispersive. This suggests that they were generated on discontinuities. On the shallow events stack (figure 3a) these arrivals dominate the track. The value of the first arriving energy is 3.5 times higher than the background energy level at 0.5Hz. Energies are twice higher than this level for the both last arrivals at 0.35Hz and 0.4Hz, respectively. On the deep events stack (figure 3b), a fourth high energy arrival is observed around 57s. It is slightly dispersed over a 3s wide window, and its frequency content is maximal around 0.3 Hz, similar to the arrival around 65s. If we consider that the remainder of the seismogram corresponds to noise, the energy ratio of the four arrivals with respect to the maximal noise level is equal to 1.6 at 0.3Hz, 1.6 at 0.55Hz, 2 at 0.33Hz, and 1.2
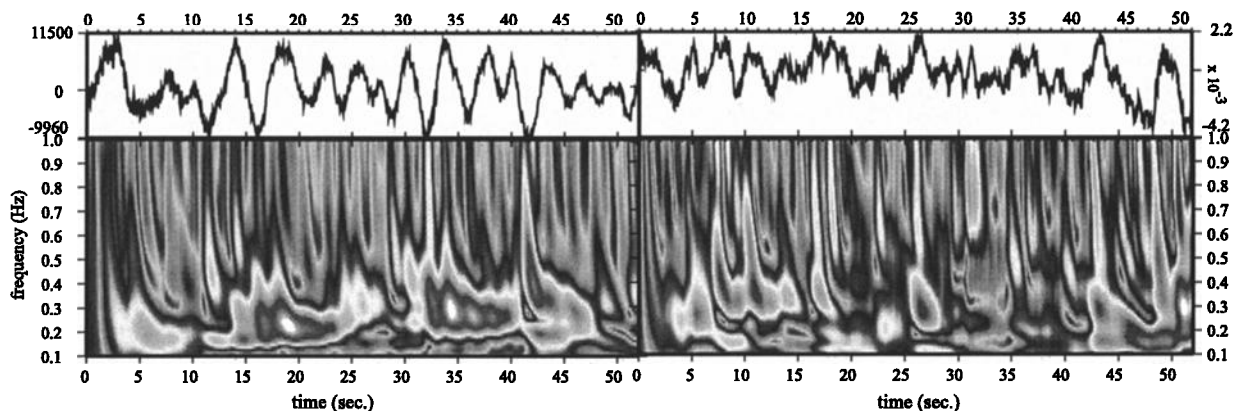

Figure 2. Effect of deconvolution on random and coherent noise. Energy diagrams of stack of seismograms recorded on the 52 invidual SV components before P-wave arrival (a) before and (b) after deconvolution. The corresponding energy scale bar is displayed in figure 3c.
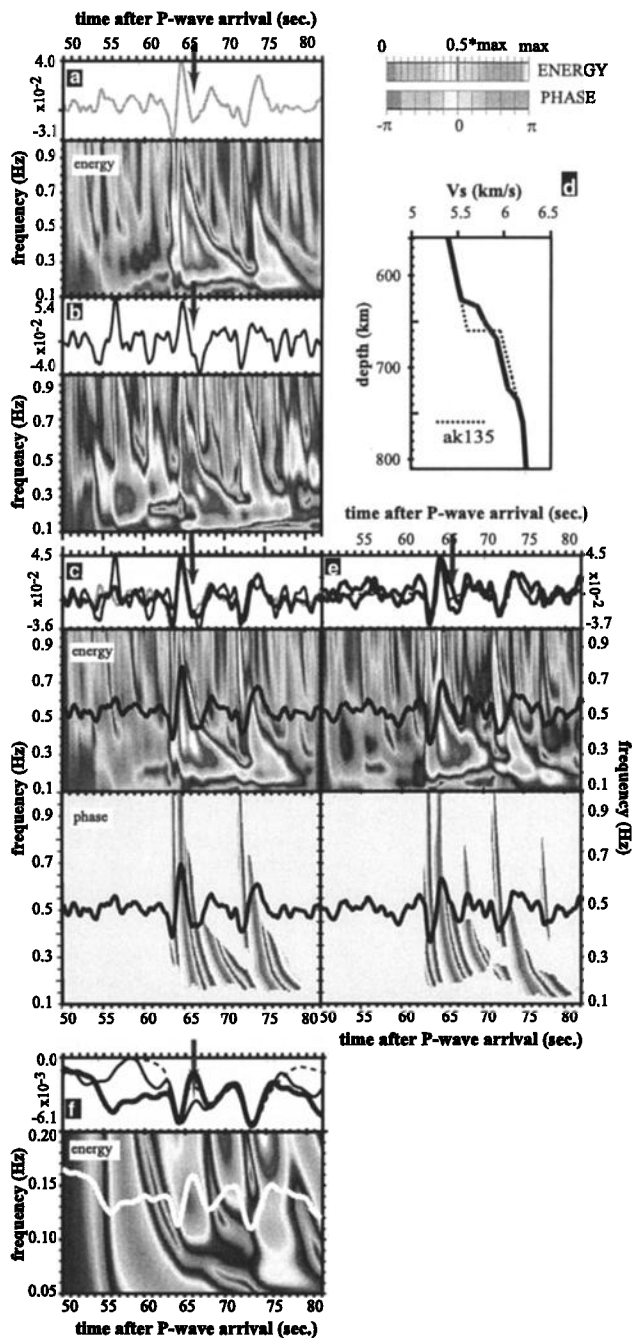
Figure 3. Wavelet transform of Californian Pds VBB records. Arrows point at the P660s phase predicted by ak135. For sake of clarity, phases are displayed only if the energy is greater than one third of the maximum energy. Amplitudes are normalized with respect to the amplitude of the P-wave. (a) 34 shallow events stack; (b) 18 deep events stack; (c) total stack (heavy solid curve). (d) Shear wave velocity profile accounting the best for the observations. (e) thin curves correspond to synthetic seismograms without (dashed curve) and with (solid curve) noise, the heavy solid curve corresponds to the total stack of figure (c); the phase and energy diagrams correspond to the synthetic seismogram. (f) total stack (heavy solid line) and noisy synthetic seismogram (thin line) filtered with a 0.167 lowpass; the phase and energy diagrams belong to the total stack. A colored version of this figure is available on the website: http://www.sciences.univ-nantes.fr/geol/UMR6112/Persnl/JCastillo/castillo.html

at 0.6Hz. These values confirm that the deep events stack is noisier than the shallow events one. Interference between noise and converted waveforms could be responsible for the differences in energy ratios between the different phases observed on each stack. The low energy ratios of the deep events stack make it difficult to discriminate between two interpretations : either the 57s, and the 66s arrivals correspond to converted phases on mantle interfaces, or the energy diagram is dominated by noise. Similarities in both stacks (figures 3a and 3b) lead one to believe that the 66s arrival is actually a converted phase on a 645km depth interface, whereas the 57s energy packet may only be associated with noise or attributed to structural complexities in the seismic source region. Figure 3c corresponds to the weighted sum of both stacks with a ratio 3:2, in order to take into account the difference of quality between both data sets. The use of the time-frequency phase diagram allows the precise recovery of the arrival time of the selected waveforms. It gives respective values of 63s, 65.2s, and 72s. A search for the best fit between the observations and WKBJ seismograms [*Chapman*, 1978] in the frequency interval 0.1-1Hz is conducted with the following unknown parameters : density, seismic velocities, and interface characteristics. The number of interfaces, as well as the initial values of their depth and thickness, are provided by the previous wavelet analysis. The ak135 parameters are left unchanged outside the investigated depth domain. Inside this domain, the total jump of parameters is distributed between the different interfaces, similarly for density and seismic velocities. Between the interfaces, ak135 velocity and density gradients remain unchanged. In the best V_S profile, shown in figure 3d, the 3 interfaces located at 625, 650 and 720km depth are 10, 18 and 13km thick, respectively. The corresponding synthetic seismogram is displayed in figure 3e. The latter has been summed with a 32s long noise series issued from figure 2b with a S/N ratio of 2, and filtered in the frequency range 0.1-1Hz. Several stacks have been produced by delaying the noise track with respect to the bare synthetic seismogram. Though we have chosen the combination that fits the best with the observations, the interference between converted phases and noise results in slightly shifting their frequency content. This effect contributes to the error on the values of interfaces' depths and thickness by the order of ± 1km.

Discussion

Dispersed waveforms generated on seismic gradients become dominant at long period, and they may hide the presence of sharp discontinuities, especially if both structures are in close proximity to one another. In fact, geodynamical interpretation based on low frequency signals, and on the assumption of a single discontinuity at the base of the upper mantle can be biased by the inadequacy between signal wavelength and investigated structure thickness. A 0.167Hz low-passed version of the total stack and its synthetics (figure 3f) shows that the three phases previously identified at higher frequencies (figure 3c) are more difficult to discriminate. When interpreted at low frequencies, this observation leads to a two-layered structure of the investigated region. Figure 3f also shows that low-pass filtering does not ensure a complete removal of the corrupting effect of microseismic noise. Care should thus be taken when interpreting seismic signals with wavelengths longer than the width of the sam-

pled interfaces. A combined use of standard deconvolution techniques and the wavelet transform allows the seismic signal to stand out from noise, and individualize arrival times of sharp phases generated on seismic discontinuities from dispersed waveforms created by gradients. The high frequency (0.1-1Hz) results obtained in the present study yield the relative depth and thickness of these structures with a better accuracy than lowpassed waveforms. Under California, we find a seismic structure which is more complex than usually observed by studies based on long-period data (e.g. *Shearer and Flanagan* [1999]. Our results are consistent with the larger scale observations of *Simmons and Gurrola* [2000] in the same region, i.e. the three interfaces located at 625, 650, and 720km depth, respectively. Our model can be viewed as a lateral average of their detailed three dimensional map of the transition zone beneath California. The main difference between both studies lies in the visibility of the 625km discontinuity, which is enhanced in our model while it is not present everywhere on a regional scale. We suspect the link between seismic interfaces and mineralogical transformations, as predicted in the laboratory, is not straightforward. For example, we obtain a thickness of about 20km for the 650km interface, while experimental studies [*Ito and Takahashi.*, 1989] predict that the transformation of ringwoodite occurs over a region less than 5km thick. The 625km discontinuity may also be a good candidate for this reaction since *Irifune et al.* [1998] have reported that it could take place at mantle pressures valid at a depth of 600km. On the other hand the 720km deep structure can be attributed more confidently to the transformation of ilmenite into perovskite, if one considers the depth range in which this transformation is likely to occur (e.g. *Vacher et al.* [1998]). The method which has been applied here proves itself to be a useful method for further observations in different geodynamical contexts and comparison with laboratory results.

References

Chapman, C.H., A new method for computing synthetic seismograms, *Geophys. J. R. astr. Soc.*, *54*, 481-518, 1978.

Chevrot, S., Vinnik, L., and J.-P. Montagner, Global patterns of upper mantle from Ps converted waves, *J. Geophys. Res., 104*, 20203-20219, 1999.

Irifune, T. N. Nishiyama, K. Kuroda, T. Inoue, M. Isshiki, W. Utsumi, K. Funakoshi, S. Urakawa, T. Uchida, T. Katsura, and O. Ohtaka, The postspinel phase boundary in Mg_2SiO_4 determined by in-situ X-ray diffraction, *Science, 279*, 1698-1700, 1998.

Ito, E., and E.Takahashi., Postspinel transformations in the system Mg_2SiO_4-Fe_2SiO_4 and some geophysical implications, *J. Geophys. Res.*, *94*, 10,637-610,646, 1989.

Kennett, B.L.N., E.R. Engdahl, and R. Buland, Constraints on seismic velocities in the Earth from traveltimes, Geophy. J. Int., *122*, 108-124, 1995.

Kumar, P., and E. Foufoula-Georgiou, Wavelet analysis of geophysical applications, *Rev. Geophys.*, *35*, 385-412, 1997.

Montagner J.-P., Where can Seismic Anisotropy be detected in the Earth's Mantle? In Boundary Layers..., *Pageoph.*, *151*, 223-256, 1998.

Moreau, F., D. Gibert, M. Holschneider, and G Saracco, Identification of sources of potential fields with the continuous wavelet transform : 1 - Basic theory, *J. Geophys. Res.*, *104*, 5003-5013, 1999.

Morlet J., G. Arens, E. Fourgeau, and D. Girard, Wave propagation and sampling theory, Parts 1 an 2, *Geophysics 47*, 203-236, 1982.

Niu, F., and H. Kawakatsu, Complex structure of the mantle discontinuities at the tip of the subducting slab beneath the Northeast China : a preliminary investigation of broadband receiver functions, *J. Phys. Earth, 44*, 701-711, 1996.

Paulssen, H., Upper mantle converted waves beneath the NARS array, *Geophys. Res. Lett., 12*, 709-712, 1985.

Shearer, P.M., and M.P. Flanagan, Seismic velocity and density jumps across the 410- and 660-kilometer discontinuities, *Science, 285*, 1545-1548, 1999.

Simmons, N.A., and H. Gurrola, Multiple seismic discontinuities near the base of the transition zone in the Earth's mantle, *Nature, 405*, 559-562, 2000.

Vacher, P., A. Mocquet, and C. Sotin, Computation of seismic profiles from mineral physics : the importance of the non-olivine components for explaining the 660 km depth discontinuity, *Phys. Earth Planet. Inter., 106*, 275-298, 1998.

Valéro, H.-P., Endoscopie sismique, PhD thesis, 256 pp., Institut de Physique du Globe at Paris France, 2000.

Vinnik, L.P., Detection of waves converted from P to SV in the mantle, *Phys. Earth Planet. Inter., 15*, 39-45, 1977.

J. Castillo and A. Mocquet, Laboratoire de Planétologie et Géodynamique, UMR-CNRS 6112, Faculté des Sciences et Techniques, 2, rue de la Houssiniere, 44300 Nantes, FRANCE (e-mail: castillo@chimie.univ-nantes.fr)

G. Saracco, Laboratoire de Géosciences Rennes, UPR 4661, Campus de Beaulieu, 263 av. du Général Leclerc, 35042 Rennes, FRANCE